Article

Neutrophil-Particle Interactions in Blood Circulation Drive Particle Clearance and Alter Neutrophil Responses in Acute Inflammation

Catherine A. Fromen, William J. Kelley, Margaret B Fish, Reheman Adili, Jeffery Noble, Mark J. Hoenerhoff, Michael Holinstat, and Omolola Eniola-Adefeso

ACS Nano, **Just Accepted Manuscript** • DOI: 10.1021/acsnano.7b03190 • Publication Date (Web): 13 Oct 2017

Neutrophil-Particle Interactions in Blood Circulation Drive Particle Clearance and Alter Neutrophil Responses in Acute Inflammation

Catherine A. Fromen[1], William J. Kelley[1], Margaret B. Fish[1], Reheman Adili[2], Jeffery Noble[1], Mark J. Hoenerhoff[3], Michael Holinstat[2,4], Omolola Eniola-Adefeso[1,5] *

1. Department of Chemical Engineering, University of Michigan, Ann Arbor, MI 48109.
2. Department of Pharmacology, University of Michigan, Ann Arbor, MI 48109.
3. *In Vivo* Animal Core, Unit for Laboratory Animal Medicine, University of Michigan, Ann Arbor, MI 48109.
4. Department of Cardiovascular Medicine, Samuel and Jean Frankel Cardiovascular Center, University of Michigan, Ann Arbor, MI 48109.
5. Department of Biomedical Engineering, University of Michigan, Ann Arbor, MI 48109.

* Corresponding author: lolaa@umich.edu

TOC Graphic

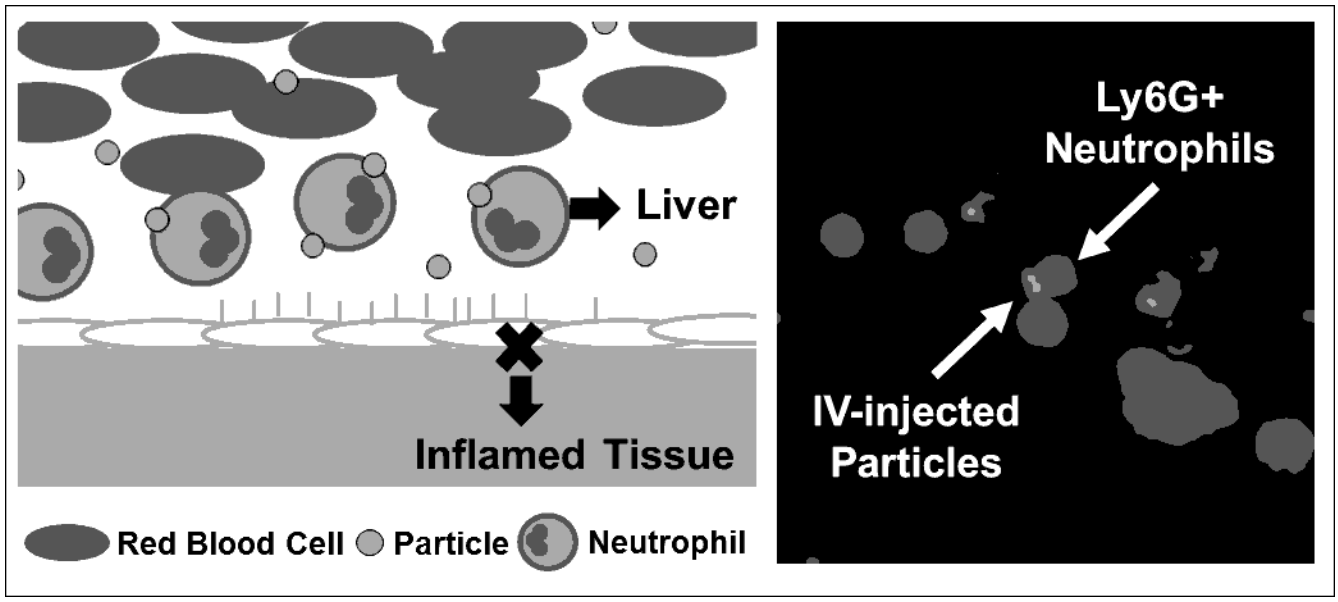
Liver
Inflamed Tissue
Red Blood Cell
Particle
Neutrophil
Ly6G+
Neutrophils
IV-injected
Particles

ABSTRACT

Although nano- and microparticle therapeutics have been studied for a range of drug delivery applications, the presence of these particles in blood flow may have considerable and understudied consequences to circulating leukocytes, especially neutrophils, which are the largest human leukocyte population. The objective of this work was to establish if particulate drug carriers in circulation interfere with normal neutrophil adhesion and migration. Circulating blood neutrophils *in vivo* were found to be capable of rapidly binding and sequestering injected carboxylate-modified particles of both 2 μm and 0.5 μm within the bloodstream. These neutrophil-particle associations within the vasculature were found to suppress neutrophil interactions with an inflamed mesentery vascular wall and hindered neutrophil adhesion. Furthermore, in a model of acute lung injury, intravenously administered drug-free particles reduced normal neutrophil accumulation in the airways of C57BL/6 mice between 52-60% *versus* particle-free mice and between 93-98% in BALB/c mice. This suppressed neutrophil migration resulted from particle-induced neutrophil diversion to the liver. These data indicate a considerable acute interaction between injected particles and circulating neutrophils that can drive variations in neutrophil function during inflammation and implicate neutrophil involvement in the clearance process of intravenously-injected particle therapeutics. Such understanding will be critical towards both enhancing designs of drug delivery carriers and developing effective therapeutic interventions in diseases where neutrophils have been implicated.

Keywords: inflammation, neutrophils, drug carriers, leukocytes, nanoparticles

Rationally designed nano- and microparticle therapeutics have been studied for a range of drug delivery applications, including cancer, atherosclerosis, and vaccines.[1-3] Somewhat surprisingly, one of the most commonly overlooked biological barriers for these intravenously (IV) administered particulate drug carriers are their physical interactions within blood. Blood itself is a complex fluid, composed of various cellular subsets. These blood cells segregate under flow into a concentrated red blood cell (RBC) core and a near-wall excess of leukocytes and platelets in the RBC free layer (RBC-FL).[4-6] For many delivery applications, particle carriers must mimic leukocyte localization and also marginate to the vessel wall to extravasate from the blood vessel.[2] Thus, the physical presence of particles in blood flow may have noticeable consequences. For one, an increased association between particles and concentrated leukocytes in the RBC-FL may escalate physical collisions and enhance clearance by circulating phagocytes, namely neutrophils ($2–8\times10^{9}$/L) and monocytes ($0.2–1.0\times10^{9}$/L).[7] Indeed, particle circulation times can be dramatically increased through depletion of circulating phagocytic cells, indicating the predominance of these leukocyte-particle interactions in the vasculature.[8] While phagocytes in general are known to contribute to the clearance of particle therapeutics, clearance is generally perceived to occur in the organs of the reticuloendothelial system (RES), including the liver and spleen.[9,10] How the colocalization of both particles and leukocytes within the RBC-FL contributes to the clearance process of IV-injected therapeutics remains unclear however.

Neutrophils (NΦ) are the largest human leukocyte population and are considered the first line of defense for the innate immune system; these cells are responsible for destroying pathogens through phagocytosis, degranulation, and formation of neutrophil extracellular traps (NETs).[11-15] These functions have been mainly studied following NΦ migration into inflamed tissue.[15] Despite the obvious potential for IV delivered particles to interact with NΦs in circulation due to their co-localization in the RBC-FL and the ability of NΦs to phagocytose foreign objects, there have been very few studies that directly probe the results of these interactions, regarding both particle efficacy and NΦ function. Countless studies have explored the biological fate of particles through *in vitro* and *in vivo* biodistribution, uptake, and efficacy studies, typically deriving therapeutic impact from the loaded active pharmaceutical ingredient (API) cargo, rather than the particle itself.[16] The limited studies exploring the impact of IV-administered particles on leukocyte function have focused on narrow leukocyte subsets. For example, recent work from Getts *et al*. demonstrated that the injection and phagocytosis of API-free, negatively charged microparticles diverted inflammatory monocytes to the spleen in a number of chronic disease models, resulting in a therapeutic benefit.[17] While this work excitingly documents how phagocyte internalization of API-free particles can impact leukocyte function and disease outcomes, the dynamics of these interactions remain largely unexplored. Notably, interaction between non-native particle entities and NΦs, the largest circulating phagocytic population, has not been investigated.

In this work, we sought to investigate the involvement of circulating NΦs with IV-injected particles. We observe that circulating NΦs, found in vasculature outside of major phagocytic organs, are capable of rapidly binding and sequestering particles. These interactions away from RES organs likely contribute to particle clearance following injection. Furthermore, we demonstrate that these associations with API-free particles in the vasculature can alter normal NΦ interactions with the vascular wall and subsequently hinder neutrophil recruitment into inflammatory tissues.

RESULTS

Circulating mouse neutrophils associate with intravenously injected particles

While previous studies have demonstrated particle association broadly with phagocytes in the vasculature outside of the RES organs of the liver and spleen,[9] we first sought to observe if neutrophils (NΦ) specifically associate with particles in circulation. C57BL/6 mice were injected with an ~30 mg/kg dosage of either 2 μm or 0.5 μm polystyrene (PS) carboxylate-functionalized (COOH) particles (corresponding to $2x10^8$ 2 μm particles or $1.28x10^{10}$ 0.5 μm particles) and whole blood obtained *via* cardiac puncture approximately 2 minutes following injection. Particles 2 μm in diameter were chosen due to their efficient margination (*i.e.* localization) in the RBC-FL,[18] as well as a prior report of microparticle interference with the functionality of inflammatory monocytes by Getts *et al*.[17] Particles of 0.5 μm were chosen as representative nanoparticle therapeutics which do not localize to the RBC-FL, but rather distribute uniformly in flow.[18] As shown in Figure 1A, mouse NΦs were identified using flow cytometry first *via* FSC vs SSC and then as CD45+CD11b+Ly6G+. Ly6G is the most commonly used surface protein for mouse NΦ identification.[12] A co-expression of CD11b, a leukocyte adhesion molecule and subunit of integrin $\alpha_M\beta_2$,[13] with Ly6G differentiates neutrophils from monocytes. From this population, particle positive NΦs were identified as FITC+ cells (Figure 1B). When dosed at equivalent mass, 11.1 ± 1.0 % of collected NΦs from mice receiving 2 μm particles were particle positive, while 35.7 ± 2.9% of collected NΦs from mice receiving 0.5 μm particles were particle positive (Figure 1C).

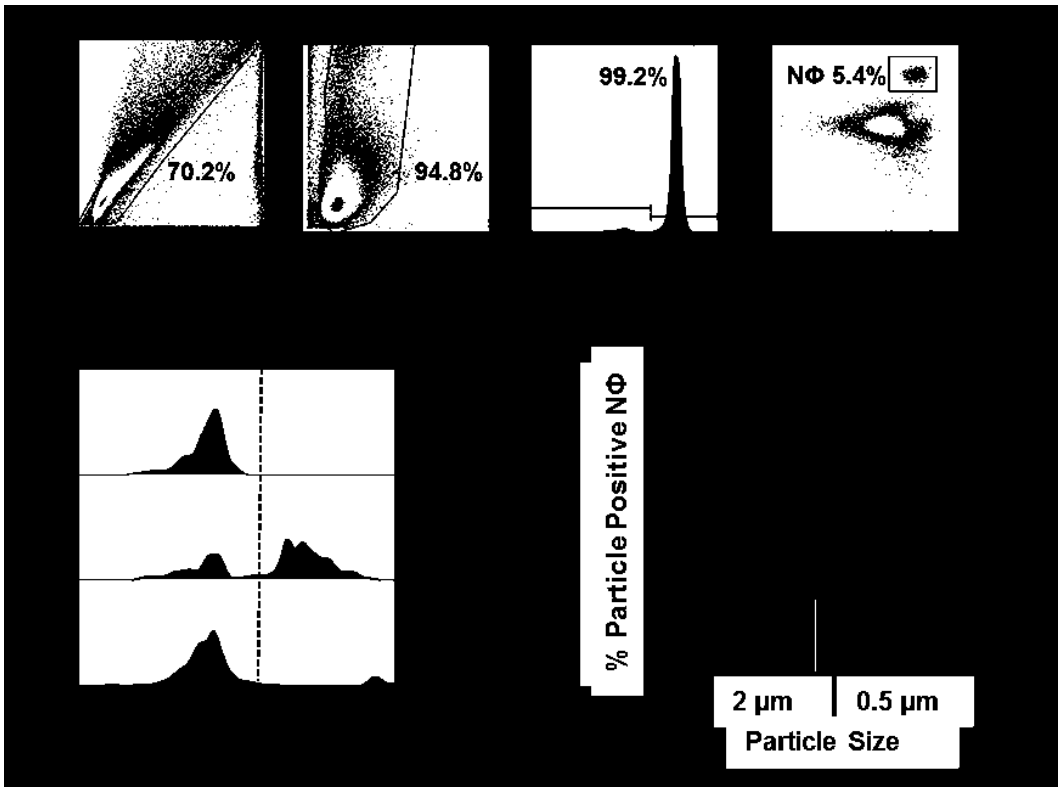

Figure 1. Neutrophil association with particles immediately following IV injection. C57BL/6 were injected with equivalent mass dosage of either 2 μm or 0.5 μm COOH particles *via* tail vein and blood was obtained within 2 minutes of particle injection *via* cardiac puncture. A) Representative gating analysis of blood sample to identify neutrophil (NΦ) population. B) Representative gating analysis and C) quantified results of particle positive NΦ in mouse blood. Graphs are representative data from a single experiment (n=3). Error bars represent standard error.

Given this measurable proportion of NΦs in circulation found to be rapidly associated with particles of both sizes, we sought to visualize these interactions live within the bloodstream. Using intravital microscopy, we visualized vasculature in the mouse mesentery and monitored rolling NΦs at the surface of an inflamed vascular wall. TNF-α was locally (topical) applied to the exposed vessel prior to particle injection to upregulate adhesive molecules and facilitate NΦs rolling, enabling us to visualize a subset of NΦs passing through the vasculature in real time. Circulating NΦs were pre-stained with anti-Ly6G and particles injected at the same equivalent mass dosage as before. As shown in Figure 2, both 2 μm and 0.5 μm particles were found associated with rolling NΦs (see Supplemental Video 1 and 2 for representative injection of 2 μm and 0.5 μm particles and Supplemental Figure 1 for a representative lower magnification of the mesentery vessel). Arrows indicate Ly6G+ NΦs that were found with particles for at least three consecutive frames, indicating that particles are firmly associated with the cell. Interestingly from these observations, we can identify NΦ which have bound both single or multiple particles. Both particle sizes were found associated specifically with NΦ populations outside of the RES

organs, indicating that NΦs in the periphery are involved in binding particles and likely contribute to clearance of IV-administered particles.

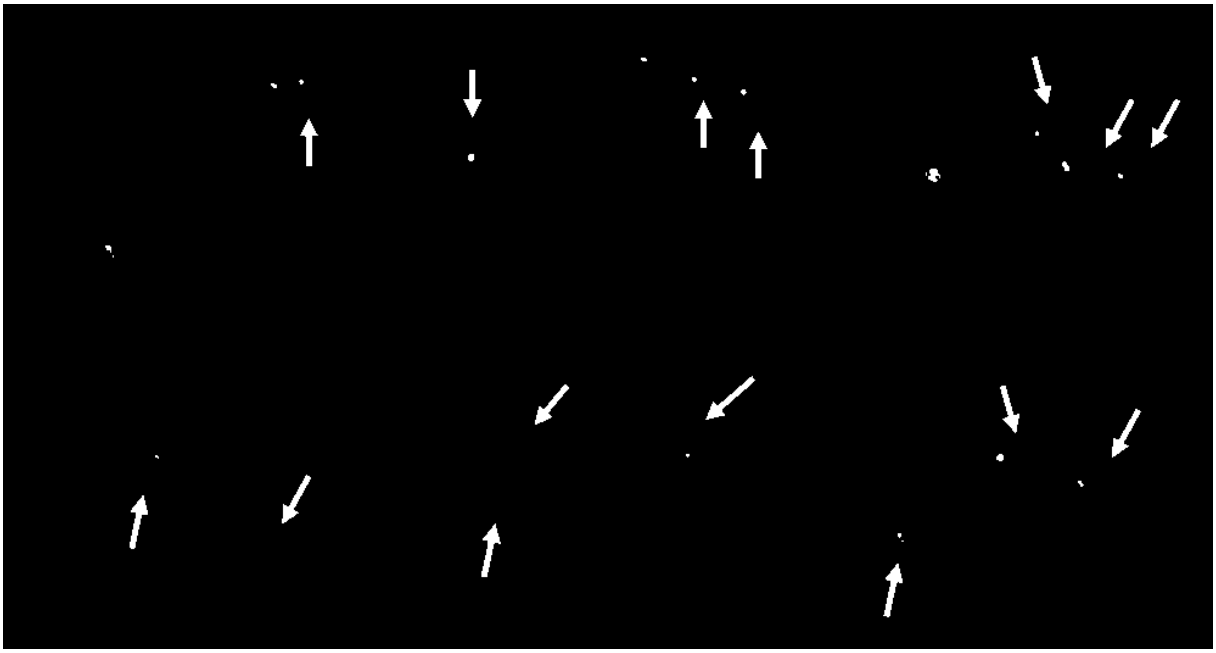

Figure 2. **Particles in circulation associated with Ly6G+ neutrophils.** Mesentery vasculature of C57BL/6 mice injected with equivalent mass dosage of either A) 2 μm or B) 0.5 μm COOH particles (green). NΦ stained with anti-Ly6G-APC (red) prior to injection and topical TNF-α applied locally to enable visualization of rolling NΦ. Arrows indicate NΦ and particles associated for at least three consecutive frames of imaging.

Particles in blood flow reduce neutrophil adhesion at an inflamed vascular wall

During our intravital investigation, we noted that the presence of particles in circulation appeared to reduce neutrophil adhesion at the vascular wall over time. To quantify this change, we assessed NΦs adhesion over time in a previously established model of acute murine mesentary inflammation.[19,20] Following the dosing schedule shown in Figure 3A, NΦ populations were quantified following 0.5 μm and 2 μm particle injection. In addition to the COOH 2 μm PS particles, we also evaluated 2 μm PS particles functionalized with a high density PEG coating (brush conformation). As discussed elsewhere[21-23] and confirmed in Supplemental Figure 2, high density PEG coatings mitigate cell uptake in mice, allowing us to confirm that any change in localization to the vessel wall would be an impact of particle internalization. TNF-α was topically applied to mesenteric veins to induce local, rapid NΦ accumulation on the vessel wall. As shown in Supplemental Figure 3, few NΦs were observed in untreated vessels, while topical administration of TNF-α resulted in rapid recruitment of NΦs. We visualized an average of over 20 NΦs on TNF-α treated vessels after 3 minutes, more than double number found after the first

minute following TNF-α application. This increased number of NΦs was maintained for the duration of the experiment in mice receiving only topical TNF-α, confirming a local inflammatory event in the vessel. Particles were injected following 3 mins of inflammation; representative images of the vessel wall following particle injections are shown in Figure 3B. Average NΦ numbers were quantified in the first minute following particle injection (3-4 minutes after TNF-α) and at subsequent (4-7 min after TNF-α) time points.

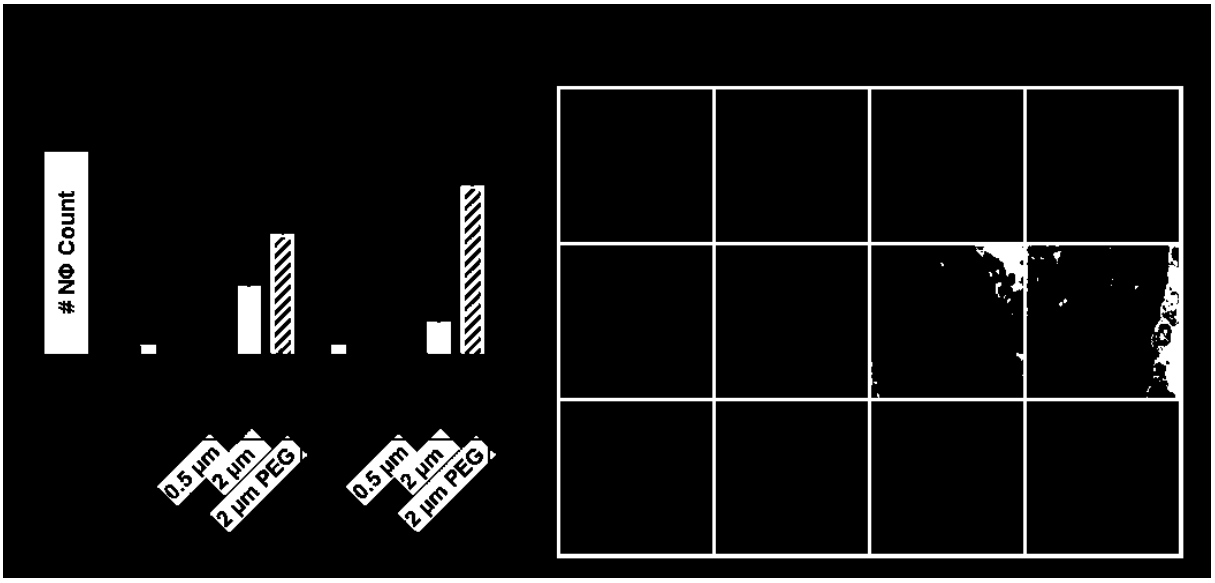

Figure 3. **Acute mesentery inflammation.** A) Dosing schedule of acute mesentery inflammation model in C57BL/6 mice. Mice received topical TNF-α at time 0 and a particle injection at 3 minutes. B) Representative images shown at 8 minutes with NΦs labeled red and particles labeled green and C) quantified results of NΦ frequency at the vascular wall following particle administration of 0.5 μm and 2 μm COOH particles or 2 μm PEGylated particles *via* IV injection. Results averaged over two ranges of time points. The top image in B shows the merge of both red and green channels, with the individual colors split below. Average NΦ counts were quantified during the first minute following particle injection (3-4 min) and longer time points (4-7 min). (*) Indicates significant difference in cell counts relative to the corresponding TNF-α only value. Statistical analysis was performed using two-way ANOVA with Sidak's multiple comparison test to TNF-α group with $\alpha = 0.01$. Bars represent averages from at least 8 different vessels within groups, n≥4 mice per group and error bars represent standard error.

In the first minute following injection, both COOH 0.5 μm and 2 μm particles produced an immediate and significant reduction in NΦ localization *versus* particle free TNF-α only vessels and continued to do so for more than four minutes (Figure 3C). NΦ localization following COOH particle injections were not statistically different than untreated vessels at either time point evaluated and resulted in about 80% reduction *versus* the TNF-α group between 4-8 minutes (78% for 0.5 μm and 83% for 2 μm, non-significant from each other). In contrast, the 2 μm PEG particles failed to result in any reduction to the NΦ localization to the vessel wall for the duration of the experiment. PEG particles were still found circulating in high quantities following 7 minutes, in comparision to both of the COOH particles which

had been largely cleared from circulation (Figure 3B bottom). The rapid decrease in NΦ adhesion following COOH administration and minimal impact of PEG administration indicates that particle uptake by NΦs may hinder normal NΦ function during inflamation.

To confirm that the observed effect was a direct impact of particle interactions with NΦs, we performed an *in vitro* parallel plate flow chamber assay (PPFC) using freshly isolated human NΦs.[18-20] Human NΦs are used due to the difficulty of isolating and obtaining a measurable quantity of mouse NΦs. As shown in Supplemental Figure 4, we observed that NΦs pre-incubated with particles reduced overall NΦ adhesion to an inflamed endothelial monolayer in a realistic flow profile as compared to samples perfused immediately after addition of particles. This trend held true for both particle sizes, with a 2 hr incubation resulting in a 30-45% reduction in NΦ adhesion from particle-free controls at the particle concentrations tested. The continued viability of the NΦs was confirmed at this time point, suggesting that particle uptake by NΦs occurring during the preincubation period and not NΦ death impacted NΦ adhesive abilities. Combined with the intravital findings, these results demonstrate that particle administration can prevent normal NΦ capture and adhesion at the vessel wall.

Reduction of neutrophil airway accumulation in an ALI model.

A critical function of NΦs are their ability to rapidly respond to proinflammatory signals and emigrate from the blood into inflammatory tissues.[11-13, 15] We sought to explore if NΦ-particle interactions would impact the normal migratory NΦ function by assessing NΦ transmigration in an acute lung injury (ALI) model.[24] ALI was induced *via* lipopolysaccharide (LPS) instillation into mice lungs, causing recruitment of NΦs to the airspace *via* increased expression of inflammatory cytokines and chemokines.[5, 24,25] Notably, LPS instillation alone does not result in significant emigration of monocytes at early time points, allowing us to isolate the evaluation of emigrating neutrophils.[26,27] One hour after LPS instillation, we administered 2 μm and 0.5 μm particles at equivalent mass *via* IV-tail vein injection to both C57BL/6 and BALB/c mice as in Figure 4A. BALB/c mice were evaluated in addition to C57BL/6 mice as they are known to demonstrate increased NΦ response to instilled LPS[24] as well as rapid particle internalization compared to C57BL/6 mice.[8] To assess NΦ migration, we evaluated the total cells in the bronchoalveolar lavage fluid (BALF) (Supplemental Figure 5), the percentage of NΦs in the BALF (Figure 4B), and the total BALF NΦ counts (Figure 4C and 4D, representative gating Supplemental Figure 5B). As shown in Figure 4B-D, mice receiving only LPS demonstrated increased BALF infiltrates, with NΦs counts averaging $1.1x10^6 \pm 1x10^5$ that corresponded to over 46% of the collected cells in C57BL/6 mice; in BALB/c mice, BALF NΦs counts averaged $3.3x10^7 \pm 1x10^7$, corresponding to over 67%. The BALF NΦs counts following an LPS administration in both mouse strains indicate occurrence of an acute inflammatory event and correspond to previous findings that BALB/c mice are more sensitive to LPS

instillation than C57BL/6. However, upon IV particle injections, the percentage of BALF NΦ and the total number of NΦ infiltrates decreased in both mouse strains. In C57BL/6 mice, ALI mice receiving 2 μm particles had total BALF NΦ counts of $5.2x10^5 \pm 2x10^5$, representing a 52% decrease from the LPS-only group and corresponding to only 37% of collected cells. Similarly, ALI mice receiving 0.5 μm particles had total BALF NΦ counts of $4.5x10^5 \pm 1x10^5$, representing a 59% decrease from the LPS-only group and corresponding to only 41% of collected cells. In BALB/c mice, the results were more pronounced. ALI BALB/c mice receiving 2 μm particles had total BALF NΦ counts of $2.9x10^6 \pm 2x10^6$, representing a 93% decrease from the LPS-only group and corresponding to only 31% of collected cells. Similarly, ALI mice receiving 0.5 μm particles had total BALF NΦ counts of $6.4x10^5 \pm 5x10^5$, representing a 98% decrease from the LPS-only group and corresponding to only 32% of collected cells. Both particle treated groups were non-statistically different than the untreated mice in both mouse strains.

Given that particle treatment resulted in a dramatic decreased accumulation of BALF NΦs, we evaluated the number of circulating NΦ present in blood at the time of harvest (Figure 4E and 4F). We observed no variation in the concentration of NΦs in the C57BL/6 mice (Figure 4E), but did observe a NΦ increase in LPS-only treated BALB/c mice, which was significantly higher than ALI mice receiving particles or untreated mice. In these mice, particle treatment decreased the number of circulating blood NΦs from an average of 2.09 ± 0.9 K/μL for LPS-only mice, to concentrations of 0.45 ± 0.2 K/μL and 0.71 ± 0.8 K/μL, for 2 μm and 0.5 μm ALI groups, respectively. NΦ concentrations in particle treated groups were not significantly different from the untreated mice. To evaluate if a particle administration still did not impact the total numbers of circulating NΦs during a period of elevated NΦ response to this tissue-specific inflammatory event, we evaluated NΦ blood concentrations following sequential blood draws following particle injection. As shown in Supplemental Figure 6, LPS treatment alone caused elevated circulating NΦs in BALB/c mice, while particle treatment appeared to suppress this response, in line with the endpoint blood results shown in Figure 4F. Significant increase in the NΦ concentration were observed for the LPS-treated mice at 30 and 60 mins, while NΦ concentrations in ALI mice receiving 2 μm particles remained consistent to the original baseline values. Likely, additional NΦs were released from a reservoir in the bone marrow during the ALI model, which is known to occur during inflammatory events.[15]

Thus, in the heightened inflammation of BALB/c mice, particle administration of both particle sizes decreased the number of circulating NΦs in the blood during ALI inflammation, in addition to reducing the number of infiltrating BALF NΦs. Evaluation of the BALF inflammatory cytokines after 2 μm particle treatment again in BALB/c mice, including IL-6, TNF-α, and albumin, which is indicative of lung permeability, indicated no statistical difference between treatment groups (Supplemental Figure 7). Taken in combination with the variation with NΦ concentrations in the blood, these results imply that the

chemoattractive signal for NΦ blood emigration remained present, but rather the decreased availability of NΦ in the blood was the main driver for decreased numbers of BALF NΦs. Likely, particle clearance by NΦs accounts for this decreased availability and occurs in both mouse strains; however, the overall dampened response to LPS in the C57BL/6 mice did not result in increased NΦs in the blood of LPS-only groups (Figure 4F).

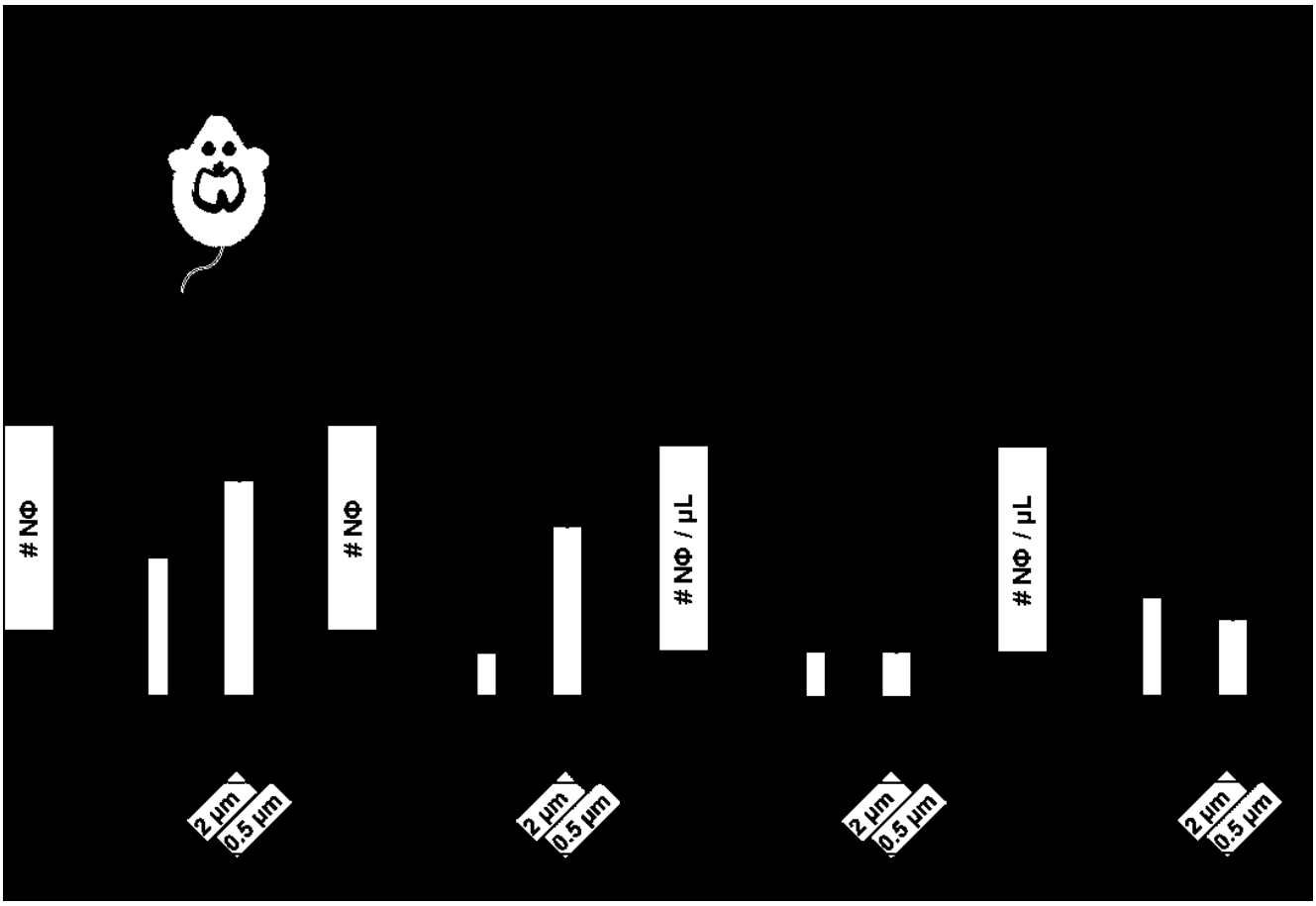

Figure 4. **Neutrophil distribution in ALI model.** A) Diagram and dosing schedule of ALI model performed in both BALB/c and C57BL/6 mice. B) Average BALF distribution of NΦ and macrophage populations (MΦ) following particle injection. Total BALF NΦ counts in C) BALB/c and D) C57BL/6 mice. NΦ concentrations from the blood following particle injection in E) BALB/c and F) C57BL/6 mice. Statistical analysis was performed using one-way ANOVA with Tukey's multiple comparison test, (**) $p<0.01$, (***) $p<0.001$, n.s. non-significant. BALF NΦ counts and blood NΦ distributions from representative single experiment (n=5). Error bars represent standard error.

To further explore the relevance of these results to drug delivery vehicles, we also evaluated 2 μm PEGylated particles in BALB/c mice in the ALI model. As shown in Supplemental Figure 8, emigrating BALF NΦs were reduced following PEGylated particle administration to the same degree as COOH particles. Furthermore, we decreased the dosed particle concentration of the 2 μm COOH particles by half to $1x10^8$, finding again a similar decrease in BALF NΦs following particle administration (Supplemental

Figure 8). Thus, the trends demonstrated in Figure 4 likely apply to a range of particle surfaces and concentrations beyond those presented here.

IV administration of particles diverts neutrophils to the liver

We next evaluated NΦ distribution in the lung, liver, and spleen, by histopathology and flow cytometry to explore if NΦ localization increased in these organs, which may account for the observed reduction of both circulating and BALF NΦs. While no differences between NΦ distributions were observed in the lung tissue or spleen (Supplemental Figure 9), we did find notable NΦ differences in the liver by both methods. As shown in the representative immunofluorescence images of liver histology sections of C57BL/6 mice (Figure 5), an increase in Ly6G+ NΦs (red) was observed in all ALI mice over the untreated groups, with further increases in both particle-ALI groups over the LPS-only controls. As corroborated in hematoxylin and eosin (H&E) stained micrographs in Supplemental Figure 10, liver sections demonstrated increased NΦ infiltrates within the hepatic sinusoids of ALI particle groups, which were mild and multifocal within affected livers without evidence of hepatocellular injury.

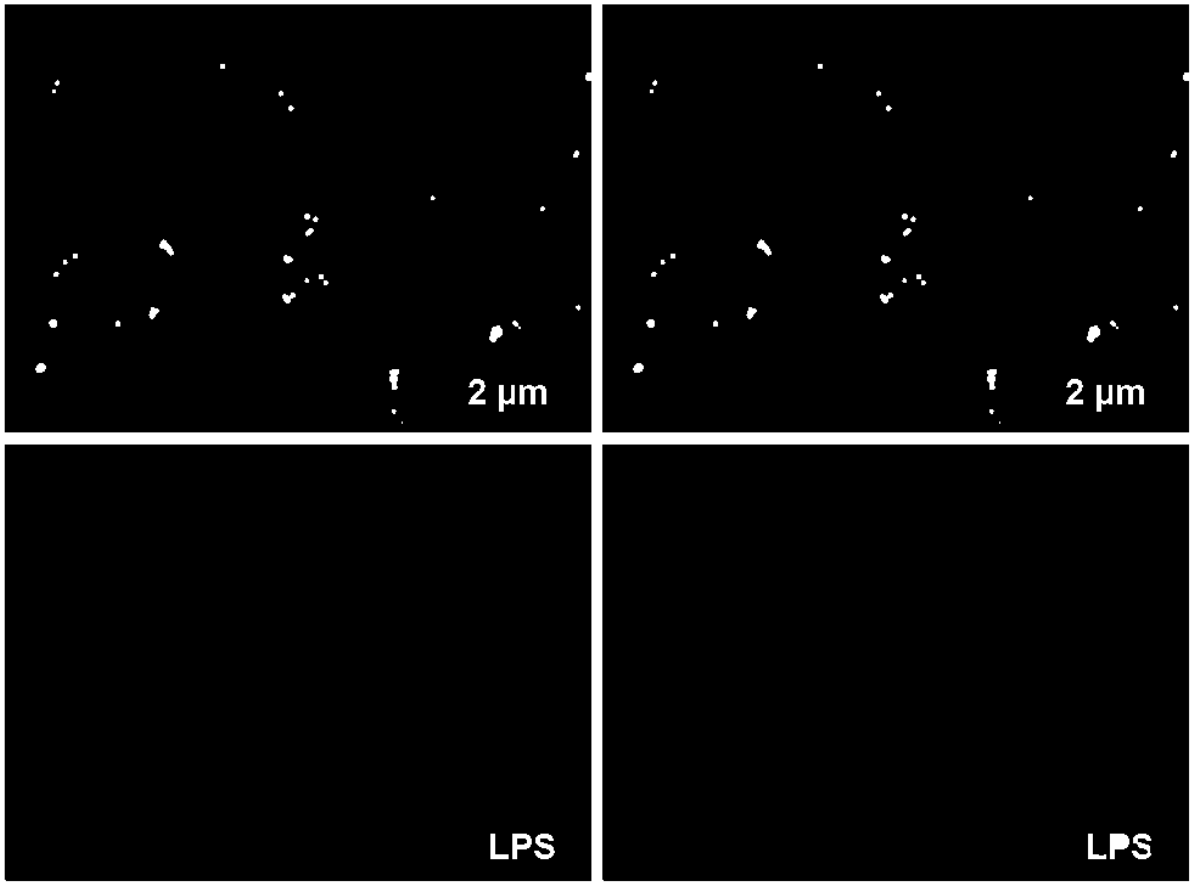

Figure 5. Representative immunofluorescence images of ALI liver histology sections. 4 μm liver sections from C57BL/6 ALI mice as in Figure 5. Particles indicated in green and Ly6G+ NΦs indicated in red. Image taken at equivalent exposure time at 40x magnification, scale bar 20 μm.

To quantify these findings, flow cytometry was used to evaluate NΦ populations in single cell liver suspensions (Figure 6, representative gating in Supplemental Figure 9). The percentage of $CD45^+CD11b^+Ly6G^+$ NΦs in the liver was significantly increased in 2 μm and 0.5 μm particle treated ALI groups compared to LPS-only and untreated mice in both mouse strains (Figure 6A and B). While LPS-only ALI mice maintained NΦ levels of roughly 10% of collected CD45+ liver cells in both mouse strains, the NΦ populations of the liver in the ALI particle groups were significantly increased. C57BL/6 mice exhibited a mild increase to 14 ± 2% and 14 ± 3% for 2 μm and 0.5 μm groups, respectively. Corresponding to the more robust response of the BALB/c mice in both LPS-sensitivity and phagocytic ability, NΦ populations of the liver of these mice increased to 33 ± 18% and 33 ± 12% for 2 μm and 0.5 μm groups, respectively. In both mouse strains, these ALI particle groups were significantly larger than both the untreated and LPS-only groups.

These findings prompted us to further explore NΦ association with particles in the liver, performed at both the whole organ and cellular level. As expected, analysis of whole organ distribution showed a considerable degree of overall particle clearance in the liver (Supplemental Figure 11). As shown in the representative immunofluorescence liver histology sections of Figure 6, we observe colocalization between Ly6G+ NΦs (red) and particles (green) throughout both the 2 μm and 0.5 μm ALI groups (Supplemental Figure 12 for annotated image). Just as frequently, we observe particles not associated with Ly6G+ NΦs. H&E stained sections of the liver suggests particle can also be found within the cytoplasm of Kupffer cells and possibly free within sinusoidal spaces (Supplemental Figure 10).

Probing at the cellular distribution within the liver with flow cytometry (Figure 6C and D), we find statistically equivalent particle uptake between CD45+CD11b+Ly6G+ NΦs and CD45+CD11b+Ly6G- macrophages (MΦ) for both particle sizes in both mouse strains (Figure 6C and D). While not statistically significant, NΦs were found associated with slightly more particles than MΦs in C57BL/6 mice; 23% or 35% NΦs were identified as particle positive while only 11% or 16% MΦs were identified as such in the 2 μm and 0.5 μm ALI groups, respectively. In BALB/c ALI 2 μm mice, 3-4% of either NΦs or MΦs were identified as particle positive; in 0.5 μm treated LPS mice, 24-25% of either NΦs or MΦs were identified as particle positive. Differences between the two particle sizes are attributed to the difference in number dose.

Finally, we explored whether protein changes on the NΦs or secreted within the liver of ALI mice following 2 μm particle administration contributed to NΦ recruitment to the liver. As shown in Supplemental Figure 11, relatively minimal fold change differences (less than 1-fold for all) in liver NΦ

expression of either CD11b or CD62L were observed across LPS-only and ALI particle groups. No changes in either of these phenotypic markers could be correlated to the increased NΦ accumulation in the liver following particle treatment. However, evaluation of inflammatory cytokines and chemokines in liver homogenates, including TNF-α, CXCL-1 KC, and CXCL-2 MIP-2 (Supplemental Figure 13) found increased production in the LPS-only group compared to the ALI 2 μm particle group or untreated mice. As in the circulating blood NΦ concentrations, 2 μm particle treatment in LPS-treated mice suppressed or prevented the inflammatory response as indicated by these cytokine/chemokine levels.

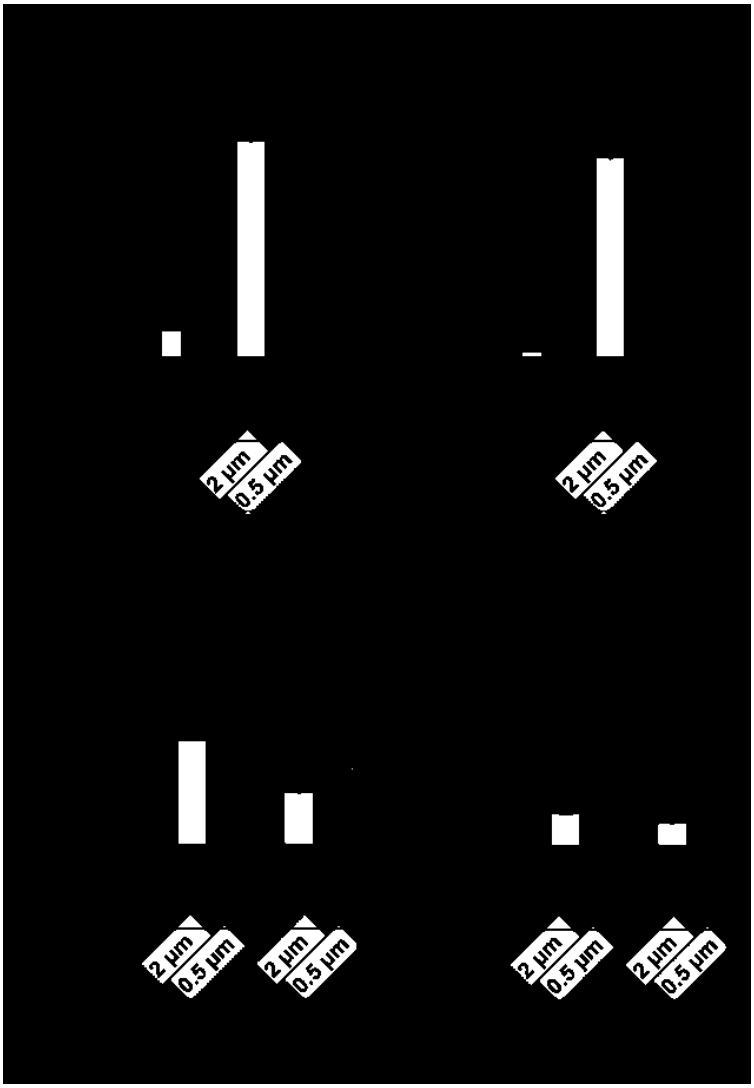

Figure 6. **Flow cytometry evaluation of liver in ALI mice.** NΦ populations of CD45+ cells in the liver following 2 μm and 0.5 μm COOH particle injection in A) C57BL/6 and B) BALB/c mice. Cellular distribution of 2 μm and 0.5 μm particles in the liver of C) C57BL/6 and D) BALB/c mice in ALI model. Statistical analysis for % NΦ population was performed using one-way ANOVA with Tukey's multiple comparison test to untreated, (*) $p<0.05$, (**) $p<0.01$. Representative results from single experiment (n=5 mice). Error bars represent standard error.

DISCUSSION

Despite the strong emergence of IV administrated micro- and nanoparticle therapeutics, major gaps remain in our understanding of how these foreign objects interact with blood cells in circulation. Here, we report that IV administration of API-free particles results in rapid association with circulating NΦs, as evidenced in collected whole blood samples (Figure 1) and visualized NΦs at the vascular wall (Figure 2). Furthermore, these associations between NΦs and API-free particles can interfere with normal NΦ function in inflammatory environments, hindering normal adhesion of circulating NΦ on an inflamed mouse mesentery wall (Figure 3) and mitigating NΦs accumulation into the inflamed mouse lung tissue (Figure 4).

The results presented here indicate a direct interaction between IV injected particles and circulating NΦs, which impacts the clearance of both entities. Indeed, these interactions do not happen in isolation. Other cellular actions are influential in the removal of both neutrophils and particles, with circulating monocytes also capable of internalizing particles[17], particle clearance occurring in the RES organs[9], and various other cell subsets contributing to cytokine and chemokine profiles responsible for cellular homing occurring after a particle interaction.[5,28] However, key observations indicate that the direct interaction between NΦs and particles are essential to clearance. In the ALI model, NΦs are diverted from the airspace only in the presence of IV-administered particles regardless of the sustained NΦ-homing cytokine signals observed in the BALF (TNF-α and IL-6, Supplemental Figure 7), which would be expected to maintain NΦ recruitment to the airspace. Furthermore, NΦ were diverted to the liver despite the decreased NΦ-homing cytokine signals in the liver (TNF-α, MIP-2, and KC, Supplemental Figure 13), which should not increase NΦ populations in the liver. These data imply that the observed interactions between particles and NΦs are impacting individual NΦ responses to drive changes in localization that are independent of existing soluble cues. Moreover, the short timescale, within minutes, of this interaction and NΦ adhesion reduction (demonstrated in Figures 1-3) likely precludes any significant change to NΦ-homing cytokines that may be secreted by other cell types, which might otherwise be hypothesized to contribute to the observed decrease in NΦ adhesion (Figure 3). Furthermore, the adhesion of isolated human NΦs to an inflamed endothelium *in vitro* was impaired by preincubation with particles (Supplemental Figure 4), further directly implicating the NΦ-particle interaction, as all other aspects of NΦ recruitment were held constant. Thus, the interaction between NΦs and particles following injection clearly drives NΦ response.

Our data suggest that multiple mechanisms contribute to NΦ diversion to the liver in the ALI model. As the liver is known to clear both IV-administrated particles[9] and apoptotic NΦs[11, 14,15], NΦ diversion may occur by the following: 1) particles are first captured in the liver through phagocytosis by resident MΦs (Kupffer cells) which then recruit circulating NΦs through elaboration of various cytokines, or 2) NΦs first phagocytose particles in the systemic circulation, triggering NΦ apoptosis and

subsequent localization to the liver for elimination, or 3) a combination of both mechanisms. Kupffer cells are known to elaborate proinflammatory cytokines to recruit inflammatory cells, including NΦs[28], and also can phagocytose dying NΦs through a P-selectin-mediated response using phosphatidylserine-dependent mechanisms.[15] In the liver, we found equivalent percentages of particle bound MΦs and NΦs (Figure 6) and equivalent NΦs expression of CD11b and CD62L (Supplemental Figure 11) across treatment groups, which are indicative markers of NΦ activation and liver homing on NΦs[13, 29-32]; taken together, these observations failed to lend insight into the driving mechanism for NΦ localization to the liver. However, we did observe suppressed production of inflammatory cytokines, including TNF-α, KC, and MIP-2, in the liver homogenate of particle-treated ALI mice (Supplemental Figure 13). Previous studies investigating systemic bacteria clearance indicated that the sequential involvement of Kupffer cell bacterial capture, NΦ immigration and phagocytosis, and subsequent NΦ apoptosis reduces proinflammatory liver cytokine production[33,34], similar to the observations presented here. In line with these results, apoptotic NΦs are known to have an anti-inflammatory impact on Kupffer cells and can drive a pro-resolution environment.[11, 35,36] These in sum may account for the suppressed inflammatory cytokine production, decreased circulating NΦs, and diminished migration to the inflamed airway in our ALI studies. Furthermore, recent work has demonstrated that the flow dynamics within the liver support passive particle capture[10], lending support to the hypothesis of initial Kupffer cell particle capture in the liver followed by NΦ recruitment. However, observations from Figure 1 and 2, which clearly identify particle association with circulating NΦs, indicate that NΦ phagocytosis of IV-administered particles occurs rapidly throughout the blood stream (within minutes). Our work demonstrates that NΦs in the periphery are capable of binding both 2 and 0.5 μm particles; combined with work by Jones *et al*., who demonstrated uptake of smaller nanoparticles by blood leukocytes in the vasculature, this further supports peripheral particle capture by NΦs and subsequent NΦ homing to the liver.[8] Additional *in vitro* PPFC assays demonstrated that isolated NΦs which interact with particles are unable to adhere to inflamed HUVEC endothelial cells, again suggesting a change to the NΦ in the periphery could prevent adhesion at the inflamed vascular wall and drive liver accumulation. Thus, our results suggest that both mechanisms contribute to the observed NΦ liver accumulation; future studies are needed to further elaborate the exact contributions of each of these mechanisms following particle injection.

Regardless of the location of where NΦs first interact with particles, our results indicate that NΦ phagocytosis is involved in the clearance of IV-injected particles. A greater decrease in BALF NΦ was observed for the BALB/c mice than the C57BL/6, in line with previous work demonstrating that BALB/c mice have more rapid particle clearance times due to enhanced phagocyte function in Th2 strain mice.[8] The particles studied here were carboxylate-modified particles, which are known to exhibit poor circulation times and rapid clearance.[21] This is attributed to specific protein absorption forming a protein

corona, which facilitates cellular internalization.[37,38] Indeed, most therapeutic drug particle designs include a brush coating of PEG to delay internalization and extend circulation times, although these particles are still cleared through the RES system.[21, 39] Our results in Figure 3 demonstrate that PEGylated particles did not hinder NΦ presence at the vascular wall, likely due to a lack of NΦ internalization of particles during this time point. This contrasts with the results of the rapidly internalized COOH particles in this model. However, the NΦ-particle mechanisms observed with the COOH particles in both models also eventually occurred with PEGylated ones. Given longer timepoints to facilitate interactions between particles and NΦs, PEGylated particles will still be cleared in part by NΦ-mediated phagocytosis, as a protein corona still is able to form on these particles prompting recognition by phagocytes.[39] Thus, the PEGylated particles in the ALI model were also capable of reducing the BALF NΦ emigration. As such, the role of NΦs in particle clearance of all types should not be over-looked. Future work will include assessment of whether other non-fouling particle surface coatings with demonstrated functional superiority over PEG, such as zwitterionic coatings[40,41], would be beneficial in eliminating the negative impact of particles on neutrophil adhesion.

CONCLUSIONS

The work presented here importantly indicates that the phagocytic prowess of circulating NΦs represents both a potential obstacle and an untapped opportunity for particulate therapeutics. Thus, improved understanding of particle-NΦ interactions will not only aid in improved designs of drug delivery carriers to optimize the particle efficacy while avoiding potentially harmful impacts on NΦs, but may also offer an opportunity to specifically manipulate neutrophil functions in numerous diseases where NΦs have been implicated.[15, 35,36] Indeed, rampant and abnormal recruitment of NΦs are common in the pathogenesis of many serious diseases, including atherosclerosis,[14, 32, 42] sepsis,[32] ischemia/reperfusion (I/R),[43] ALI,[43,44] cystic fibrosis,[45] and cancer.[46] However, more work is needed to explore the extent of particle-NΦ interaction and long-term effects, including the restoration of normal NΦ recruitment, the impact of particle delivery on subsequent infection, and the consequences of NΦ liver accumulation. Ultimately, increased knowledge of the interactions between NΦs and particles in circulation will enable successful translation of rationally designed particle therapeutics to the clinic.

METHODS

Study Approvals

Animal studies were conducted in accordance with NIH guidelines for the care and use of laboratory animals and approved by the Institutional Committee on Use and Care of Animals (ICUCA) at

the University of Michigan. All animals were maintained in pathogen-free facilities at the University of Michigan and used between 3-8 weeks in age, with study groups randomized across housing.

Particle functionalization and fabrication

Fluorescent carboxylated (COOH) polystyrene (PS) particles of 2 μm or 0.5 μm in diameter were purchased containing either a green (fluorescein isothiocyanate, FITC, Polysciences) or near-infrared (Phosphorex) fluorophore. Stock concentrations of all particles were tested for endotoxin contamination using a chromogenic LAL assay (Genscript) and confirmed injected doses were approximated at <0.1 EU/mL. Endotoxin-free water and sterile conditions (whenever possible) were implemented throughout particle processing. To fabricate PEG modified 2 μm PS particles, particles (0.1% w/v) were washed with 50 mM MES buffer and incubated with N-(3-Dimethylaminopropyl)-N′ -ethylcarbodiimide hydrochloride (EDC, 20 mg/ml, Sigma) and methoxypolyethylene glycol amine, molecular weight 5,000 (30 mg/mL, Alfa Aesar). After incubating for 2 hr at room temperature, glycine (7.5 mg/ml, Sigma) was added for 15 mins to quench the reaction and then washed with PBS buffer containing 1% BSA and stored at 4°C until use. PEG brush density was confirmed using rhodamine PEG amine, MW 5,000 (Nanocs) as described previously[21] and in Supplemental Figure 2.

Mouse whole blood sampling and analysis following particle injection

Female C57BL/6 mice (Jackson) between 6-10 weeks in age were injected *via* tail vein with either 2 μm or 0.5 μm particles, dosed at equivalent mass. Mice received $2x10^8$ 2 μm particles or $1.28x10^{10}$ 0.5 μm in 200 μL injection volume, corresponding to ~0.6mg/mouse, ~30mg/kg. These dosages were chosen as they are within a particle mass range typically used in drug delivery preclinical mouse evaluations[21,47-49] and are appropriate to translate to human doses.[50] Blood was collected at various time points either *via* cardiac puncture or saphenous vein. Samples collected *via* cardiac puncture were collected in heparin as an anti-coagulant and immediately stained with anti-Ly6G-APC, anti-CD45-PE/Cy7, and anti-CD11b-APC/Cy7 on ice. After 30 minutes of staining, blood was treated with 1X RBC Lyse/Fix (eBioscience) following recommended protocol and analyzed *via* flow cytometry. Flow cytometry data was collected on an Attune NxT Focusing flow cytometer (Life Technologies) and analyzed using FlowJo software (Tree Star). Samples collected *via* saphenous vein for NΦ concentrations were collected in EDTA coated tubes and analyzed using a Hemavet Analyzer (Drew Scientific) Complete Blood Counter (CBC).

Inflamed Mesentery Evaluation via Intravital Fluorescence Microscopy

Female C57BL/6 mice (Jackson) between 3-4 weeks in age were evaluated in a model of mesentery inflammation as described previously.[19] Neutrophil rolling and adhesion in mesenteric veins was visualized using a 25x oil objective an inverted fluorescence microscope (Zeiss Axio Observer Z1 Marianas Microscope) using Slidebook 6 software. Mice were anesthetized and a tail vein catheter placed for delivery of reagents. Mice were placed on a custom-made microscopic heated stage at 37°C, and the mesentery was exteriorized to a glass cover slip through a midline incision. Rhodamine 6G (Rh6G, Sigma, 100 μL of 0.1 mg/mL in PBS) or anti-Ly6G (Biolegend) was injected IV and local injury was induced by topical application of TNF-α (Fitzgerald, 10 μL of 200 μg/mL in PBS). FITC labeled particles suspended in PBS were injected *via* IV catheter 3 mins following topical TNF-α application and imaged for another 7 mins. Mice received $2x10^8$ 2 μm particles or $1.28x10^{10}$ 0.5 μm in 200 μL injection volume, corresponding to ~0.6mg/mouse, ~30mg/kg. Analysis was performed using Slidebook 6 and ImageJ by a blinded investigator. Images were recorded continuously in green, red, and bright field channels every 100 ms. Vessels were chosen in each mouse based on size and vessel exposure, with the average diameter of veins ranging from 90 - 190 μm, with an average of 130 μm. Total number of NΦ and particles were counted per frame to obtain average NΦ counts per 3 s of capture in 125 μm length of mesentery vessel, corresponding to 30 frames at 100 ms/frame.[19]

Parallel Plate Flow Chamber Assay

A parallel plate flow chamber (PPFC) assay was performed to evaluate NΦ binding *in vitro*. Human umbilical vein endothelial cells (HUVEC) were isolated and cultured as described previously.[18-20] Venous blood from healthy adults was collected in heparin anticoagulant and separated using a Lymphoprep (STEMCELL Technologies) gradient. Following the centrifugal separation, monocytes and lymphocytes were discarded from the buffy-coat; NΦs and RBCs obtained in the pellet were recombined with leukocyte-free plasma collected above the buffy-coat. NΦs and RBCs in plasma were then added to particles at an equivalent mass concentration ($1x10^7$/mL 2 μm particles or $6.8x10^8$/mL 0.5 μm particles). Preincubated samples were incubated at 37°C for 2 hrs, with control particle-free samples incubated under the same conditions. Samples were then assayed over an interleukin-1β (1 ng/ml) activated HUVEC monolayer to evaluate NΦ binding as described previously.[18-20] Samples were perfused over the activated HUVEC monolayer attached to a PPFC (Glycotech) in a laminar flow profile, corresponding to a wall shear rate of 1000 s^{-1} for 5 minutes. After sample perfusion, NΦ adhesion was assessed *via* optical imaging using a Nikon TE-2000-S inverted microscope with a digital camera (Photometrics CoolSNAP EZ with a Sony CCD sensor). Results were imaged and analyzed *via* ImageJ by a blinded investigator. Each experimental data point with particles was normalized to an untreated control from the same blood donor to eliminate donor to donor NΦ variation, then averaged across donors. Cell viability of NΦs with

and without particle incubation was performed following a dextran separation from RBCs using a CellTiter Glo Luminescent Cell Viability Assay (Promega) following manufacturer's instructions.

Acute Lung Injury Model

The impact of IV-administered particles on NΦ migration was evaluated in an established model of ALI.[24,25] Male C57BL/6 and BALB/c mice (Jackson) were anesthetized using isofluorane and then lipopolysaccharide (LPS, 20 μg of LPS at 0.4 mg/mL) was delivered to the lungs through an orotracheal instillation in a 50 μL volume in PBS, as described elsewhere.[22, 51] This causes a rapid recruitment of neutrophils to the airspace.[24] One hour after instillation, mice were injected with a suspension of particles in PBS through the tail vein. Mice received $2x10^8$ 2 μm particles or $1.28x10^{10}$ 0.5 μm in 200 μL injection volume, corresponding to ~0.6mg/mouse, ~30mg/kg. Two or three hours after LPS instillation, mice were euthanized, blood collected *via* cardiac puncture in ACD, and perfused with PBS. Bronchoalveolar lavage fluid (BALF) was collected by inserting a cannula in an incision in the trachea and flushing the lungs three sequential 1 mL washes of PBS. BALF cells were obtained by centrifugation, separating BALF cells from supernatant.

Following the lavage, organs were harvested and imaged using an Odyssey CLx Infrared Imaging System (LI-COR) and whole organ scans performed. Following NIR scan, lung, liver, and spleen were homogenized into single cell suspensions as previously described[52] or frozen for histological examination. Frozen samples were imbedded in OCT (Fisher) in disposable cassettes and flash frozen with a isopentane slurry; additional liver samples were fixed in 4% paraformaldehyde (PFA)or flash frozen in liquid nitrogen and stored for histology or protein analysis.

Whole organ NIR scans

Whole organ scans were completed at 169 μm resolution using the 800 nm detection channel with NIR particles. Total fluorescence for each organ was determined by drawing a region of interest (ROI) using Image Studio Software (LI-COR). Background organ fluorescence was determined from untreated samples and subtracted from the fluorescence obtained in each organ ROI. Total recovered fluorescence was determined as the sum from each organ; the corresponding fluorescent percentage was determined as a portion of this total.

Histology

Cryosectioning, hematoxylin and eosin (H&E), and immunofluorescence staining was performed by the *In Vivo* Animal Core (IVAC) at the University of Michigan. Liver samples were sliced into 4 μm sections. Samples for immunofluorescence obtained from frozen samples and stained with primary rat

anti-mouse Ly6G antibody and rabbit anti-rat IgG H+L secondary Alexa Fluor 594 antibody (Fisher). Histopathologic examination of liver sections was blinded, assessed, and imaged by a board-certified veterinary pathologist.

Cell Isolation and Tissue Homogenates

For analysis of ALI cells, single cell suspensions of the lung and liver in the ALI model were first digested with 5 mg/mL collagenase D. All three organs were physically agitated and exposed to RBC lyse buffer. Liver and lung lymphocytes were isolated using a Lymphoprep (Stemcell Technologies) gradient and all cells then stained for flow cytometry. Cells were counted *via* hemocytometer to obtain total BALF cell numbers. Single cell suspensions of mouse cells from BALF, lung, liver, or spleen were blocked (anti-CD16/32, Biolegend) and stained with a panel of fluorescent antibodies for flow cytometric analysis of cell populations. The following antibodies were used: CD45-PE, CD45-APC/Cy7, CD11c-APC/Cy7, Ly6-G-APC, CD11b-Alexa488, CD11b-PE, CD62L-PE/Cy7, annexin V-PE, annexin V-APC (Biolegend) and SiglecF-BV515 (BD). Cells were fixed with 4% PFA in PBS after staining and kept at 4°C until analysis.

To measure cytokine concentrations in the liver, frozen tissue samples were weighed and added to T-PER extraction buffer (Thermo Pierce) containing HALT protease inhibitor cocktail EDTA free (Thermo Pierce) at 30 mg/mL. Samples were mechanically agitated and sonicated on ice and centrifuged. The lysate was evaluated *via* enzyme-linked immunosorbent assay (ELISA) for TNF-α, MIP-2, KC (R&D Systems), and IL-6 (BD) following manufacturer's instructions. Cytokine concentrations in the BALF were also evaluated *via* ELISA.

Flow cytometry data was collected on an Attune NxT Focusing flow cytometer (Life Technologies) and analyzed using FlowJo software (Tree Star).

Statistics

For all studies, all data points were included in the analyses and no outliers were excluded in calculations of means or statistical significance. Data are plotted with standard error bars and analyzed as indicated in figure legends. Asterisks indicate p values of *<0.05, **<0.01, ***<0.001 and n.s indicates not significant.

ACKNOWLEDGEMENTS

The authors acknowledge H. Safari, W. Rosenbury-Smith, K. Toy, G. Thurber, S. Bhatnagar, L. Zhang, C Cilliers, A. Golinski, and M. Braunreuther for useful discussions and technical assistance.

SOURCES OF FUNDING

This work was funded in part by an NSF CAREER grant CBET1054352 (O.E.A.), University of Michigan President's Postdoctoral Fellowship (C.A.F.), and NIH grants T32-HL-125242 (M.B.F.), R01 HL115138 (O.E.A.), HL114405 (M.H.), and GM105671 (M.H.).

SUPPORTING INFORMATION AVAILABLE: Extended characterization of the particles, mesentery inflammation, representative flow cytometry gating, additional blood subtypes, and the ALI model. This material is available free of charge *via* the internet at http://pub.acs.org.

REFERENCES

1. Torchilin, V. P., Multifunctional Nanocarriers. *Adv Drug Deliv Rev* **2006,** *58*, 1532-1555.
2. Fish, M. B.; Thompson, A. J.; Fromen, C. A.; Eniola-Adefeso, O., Emergence and Utility of Nonspherical Particles in Biomedicine. *Ind Eng Chem Res* **2015,** *54*, 4043-4059.
3. Noble, J.; Zimmerman, A.; Fromen, C. A., Potent Immune Stimulation from Nanoparticle Carriers Relies on the Interplay of Adjuvant Surface Density and Adjuvant Mass Distribution. *ACS Biomater Sci Eng* **2017,** *3*, 560-571.
4. Kumar, A.; Graham, M. D., Mechanism of Margination in Confined Flows of Blood and Other Multicomponent Suspensions. *Phys Rev Lett* **2012,** *109*.
5. Zemans, R. L.; Colgan, S. P.; Downey, G. P., Transepithelial Migration of Neutrophils: Mechanisms and Implications for Acute Lung Injury. *Am J Respir Cell Mol Biol* **2009,** *40*, 519-35.
6. Ley, K.; Laudanna, C.; Cybulsky, M. I.; Nourshargh, S., Getting to the Site of Inflammation: The Leukocyte Adhesion Cascade Updated. *Nat Rev Immunol* **2007,** *7*, 678-89.
7. Ryan, D. H., Examination of Blood Cells. In *Williams Hematology*, 8e ed.; Lichtman, M. A.; Kipps, T. J.; Seligsohn, U.; Kaushansky, K.; Prchal, J. T., Eds. McGraw-Hill: New York, 2010.
8. Jones, S. W.; Roberts, R. A.; Robbins, G. R.; Perry, J. L.; Kai, M. P.; Chen, K.; Bo, T.; Napier, M. E.; Ting, J. P.; Desimone, J. M.; Bear, J. E., Nanoparticle Clearance Is Governed by Th1/Th2 Immunity and Strain Background. *J Clin Invest* **2013,** *123*, 3061-73.
9. Nel, A. E.; Madler, L.; Velegol, D.; Xia, T.; Hoek, E. M. V.; Somasundaran, P.; Klaessig, F.; Castranova, V.; Thompson, M., Understanding Biophysicochemical Interactions at the Nano-Bio Interface. *Nat Mater* **2009,** *8*, 543-557.
10. Tsoi, K. M.; MacParland, S. A.; Ma, X.-Z.; Spetzler, V. N.; Echeverri, J.; Ouyang, B.; Fadel, S. M.; Sykes, E. A.; Goldaracena, N.; Kaths, J. M.; Conneely, J. B.; Alman, B. A.; Selzner, M.; Ostrowski, M. A.; Adeyi, O. A.; Zilman, A.; McGilvray, I. D.; Chan, W. C. W., Mechanism of Hard-Nanomaterial Clearance by the Liver. *Nat Mater* **2016,** *15*, 1212-1221.
11. Fox, S.; Leitch, A. E.; Duffin, R.; Haslett, C.; Rossi, A. G., Neutrophil Apoptosis: Relevance to the Innate Immune Response and Inflammatory Disease. *J Innate Immun* **2010,** *2*, 216-27.
12. Jhunjhunwala, S., Neutrophils at the Biological–Material Interface. *ACS Biomater Sci Eng* **2017**.
13. Mantovani, A.; Cassatella, M. A.; Costantini, C.; Jaillon, S., Neutrophils in the Activation and Regulation of Innate and Adaptive Immunity. *Nat Rev Immunol* **2011,** *11*, 519-31.
14. Nordenfelt, P.; Tapper, H., Phagosome Dynamics During Phagocytosis by Neutrophils. *J Leukoc Biol* **2011,** *90*, 271-84.
15. Summers, C.; Rankin, S. M.; Condliffe, A. M.; Singh, N.; Peters, A. M.; Chilvers, E. R., Neutrophil Kinetics in Health and Disease. *Trends Immunol* **2010,** *31*, 318-24.
16. Allen, T. M.; Cullis, P. R., Drug Delivery Systems: Entering the Mainstream. *Science* **2004,** *303*, 1818-22.
17. Getts, D. R.; Terry, R. L.; Getts, M. T.; Deffrasnes, C.; Müller, M.; van Vreden, C.; Ashhurst, T. M.; Chami, D.; McCarthy, D.; Wu, H.; Ma, J.; Martin, A.; Shae, L. D.; Witting, P.; Kansas, G. S.; Kühn, J.; Hafezi, W.; Campbell, I. L.; Reilly, D.; Say, J.; Brown, L.; White, M. Y.; Cordwell, S. J.; Chadban, S. J.; Thorp, E. B.; Bao, S.; Miller, S. D.; King, N. J. C., Therapeutic Inflammatory Monocyte Modulation Using Immune-Modifying Microparticles. *Sci Transl Med* **2014,** *6*, 219ra7.
18. Charoenphol, P.; Mocherla, S.; Bouis, D.; Namdee, K.; Pinsky, D. J.; Eniola-Adefeso, O., Targeting Therapeutics to the Vascular Wall in Atherosclerosis--Carrier Size Matters. *Atherosclerosis* **2011,** *217*, 364-70.
19. Fish, M. B.; Fromen, C. A.; Lopez-Cazares, G.; Golinski, A. W.; Scott, T. F.; Adili, R.; Holinstat, M.; Eniola-Adefeso, O., Exploring Deformable Particles in Vascular-Targeted Drug Delivery: Softer Is Only Sometimes Better. *Biomaterials* **2017,** *124*, 169-179.
20. Fromen, C. A.; Fish, M. B.; Zimmerman, A.; Adili, R.; Holinstat, M.; Eniola-Adefeso, O., Evaluation of Receptor-Ligand Mechanisms of Dual-Targeted Particles to an Inflamed Endothelium. *Bioeng Transl Med* **2016,** *1*, 103-115.

21. Perry, J. L.; Reuter, K. G.; Kai, M. P.; Herlihy, K. P.; Jones, S. W.; Luft, J. C.; Napier, M.; Bear, J. E.; DeSimone, J. M., Pegylated Print Nanoparticles: The Impact of Peg Density on Protein Binding, Macrophage Association, Biodistribution, and Pharmacokinetics. *Nano Lett* **2012,** *12*, 5304-10.
22. Shen, T. W.; Fromen, C. A.; Kai, M. P.; Luft, J. C.; Rahhal, T. B.; Robbins, G. R.; DeSimone, J. M., Distribution and Cellular Uptake of Pegylated Polymeric Particles in the Lung Towards Cell-Specific Targeted Delivery. *Pharm Res* **2015,** *32*, 3248-60.
23. Yang, Q.; Jones, S. W.; Parker, C. L.; Zamboni, W. C.; Bear, J. E.; Lai, S. K., Evading Immune Cell Uptake and Clearance Requires Peg Grafting at Densities Substantially Exceeding the Minimum for Brush Conformation. *Mol Pharm* **2014,** *11*, 1250-1258.
24. Matute-Bello, G.; Frevert, C. W.; Martin, T. R., Animal Models of Acute Lung Injury. *Am J Physiol Lung Cell Mol Physiol* **2008,** *295*, L379-L399.
25. Grommes, J.; Soehnlein, O., Contribution of Neutrophils to Acute Lung Injury. *Mol Med* **2011,** *17*, 293-307.
26. Maus, U.; Huwe, J.; Maus, R.; Seeger, W.; Lohmeyer, J., Alveolar Je/Mcp-1 and Endotoxin Synergize to Provoke Lung Cytokine Upregulation, Sequential Neutrophil and Monocyte Influx, and Vascular Leakage in Mice. *Am J Respir Crit Care Med* **2001,** *164*, 406-11.
27. Maus, U. A.; Janzen, S.; Wall, G.; Srivastava, M.; Blackwell, T. S.; Christman, J. W.; Seeger, W.; Welte, T.; Lohmeyer, J., Resident Alveolar Macrophages Are Replaced by Recruited Monocytes in Response to Endotoxin-Induced Lung Inflammation. *Am J Respir Cell Mol Biol* **2006,** *35*, 227-35.
28. Mawet, E.; Shiratori, Y.; Hikiba, Y.; Takada, H.; Yoshida, H.; Okano, K.; Komatsu, Y.; Matsumura, M.; Niwa, Y.; Omata, M., Cytokine-Induced Neutrophil Chemoattractant Release from Hepatocytes Is Modulated by Kupffer Cells. *Hepatology* **1996,** *23*, 353-358.
29. Burton, J. L.; Kehrli, M. E.; Kapil, S.; Horst, R. L., Regulation of L-Selectin and Cd18 on Bovin Neutrophils by Glucocorticoids: Effects of Cortisol and Dexamethasone. *J Leukoc Biol* **1995,** *57*, 317-325.
30. Liles, W. C.; Dale, D. C.; Klebanoff, S. J., Glucocorticoids Inhibit Apoptosis of Human Neutrophils. *Blood* **1995,** *86*, 3181-3188.
31. Fortunati, E.; Kazemier, K. M.; Grutters, J. C.; Koenderman, L.; Van den Bosch v, J., Human Neutrophils Switch to an Activated Phenotype after Homing to the Lung Irrespective of Inflammatory Disease. *Clin Exp Immunol* **2009,** *155*, 559-66.
32. Phillipson, M.; Kubes, P., The Neutrophil in Vascular Inflammation. *Nat Med* **2011,** *17*, 1381-90.
33. Gregory, S. H.; Sagnimeni, A. J.; Wing, E. J., Bacteria in the Bloodstream Are Trapped in the Liver and Killed by Immigrating Neutrophils. *J Immunol* **1996,** *157*, 2514-2520.
34. Holub, M.; Cheng, C. W.; Mott, S.; Wintermeyer, P.; van Rooijen, N.; Gregory, S. H., Neutrophils Sequestered in the Liver Suppress the Proinflammatory Response of Kupffer Cells to Systemic Bacterial Infection. *J Immunol* **2009,** *183*, 3309-16.
35. Fullerton, J. N.; Gilroy, D. W., Resolution of Inflammation: A New Therapeutic Frontier. *Nat Rev Drug Discov* **2016,** *15*, 551-67.
36. Soehnlein, O.; Lindbom, L., Phagocyte Partnership During the Onset and Resolution of Inflammation. *Nat Rev Immunol* **2010,** *10*, 427-39.
37. Pino, P. d.; Pelaz, B.; Zhang, Q.; Maffre, P.; Nienhaus, G. U.; Parak, W. J., Protein Corona Formation around Nanoparticles - from the Past to the Future. *Mater Horiz* **2014,** *1*, 301-313.
38. Ritz, S.; Schöttler, S.; Kotman, N.; Baier, G.; Musyanovych, A.; Kuharev, J.; Landfester, K.; Schild, H.; Jahn, O.; Tenzer, S.; Mailänder, V., Protein Corona of Nanoparticles: Distinct Proteins Regulate the Cellular Uptake. *Biomacromolecules* **2015,** *16*, 1311-1321.
39. Aggarwal, P.; Hall, J. B.; McLeland, C. B.; Dobrovolskaia, M. A.; McNeil, S. E., Nanoparticle Interaction with Plasma Proteins as It Relates to Particle Biodistribution, Biocompatibility and Therapeutic Efficacy. *Adv Drug Deliv Rev* **2009,** *61*, 428-437.
40. Xing, C. M.; Meng, F. N.; Quan, M.; Ding, K.; Dang, Y.; Gong, Y. K., Quantitative Fabrication, Performance Optimization and Comparison of PEG and Zwitterionic Polymer Antifouling Coatings. *Acta biomaterialia* **2017**.

41. Estephan, Z. G.; Schlenoff, P. S.; Schlenoff, J. B., Zwitteration as an Alternative to PEGylation. *Langmuir* **2011**, 27, 6794-800.
42. Libby, P., Inflammation in Atherosclerosis. *Nature* **2002,** *420*, 868-874.
43. Jordan, J. E.; Zhao, Z.-Q.; Vinten-Johansen, J., The Role of Neutrophils in Myocardial Ischemia-Reperfusion Injury. *Cardiovasc. Res.* **1999,** *43*, 860-878.
44. Grommes, J.; Soehnlein, O., Neutrophils in Acute Lung Injury. *Mol. Med.* **2011,** *17*, 293-307.
45. Conese, M.; Copreni, E.; Gioia, S. D.; Rinaldis, P. D.; Fumarulo, R., Neutrophil Recruitment and Airway Epithelial Cell Involvement in Chronic Cystic Fibrosis Lung Disease. *J Cyst Fibros* **2003,** *2*, 129-135.
46. Scapini, P.; Cassatella, M. A., Social Networking of Human Neutrophils within the Immune System. *Blood* **2014,** *124*, 710-719.
47. Reuter, K. G.; Perry, J. L.; Kim, D.; Luft, J. C.; Liu, R.; DeSimone, J. M., Targeted Print Hydrogels: The Role of Nanoparticle Size and Ligand Density on Cell Association, Biodistribution, and Tumor Accumulation. *Nano Lett* **2015,** *15*, 6371-6378.
48. Ashton, S.; Song, Y. H.; Nolan, J.; Cadogan, E.; Murray, J.; Odedra, R.; Foster, J.; Hall, P. A.; Low, S.; Taylor, P.; Ellston, R.; Polanska, U. M.; Wilson, J.; Howes, C.; Smith, A.; Goodwin, R. J. A.; Swales, J. G.; Strittmatter, N.; Takáts, Z.; Nilsson, A.; Andren, P.; Trueman, D.; Walker, M.; Reimer, C. L.; Troiano, G.; Parsons, D.; De Witt, D.; Ashford, M.; Hrkach, J.; Zale, S.; Jewsbury, P. J.; Barry, S. T., Aurora Kinase Inhibitor Nanoparticles Target Tumors with Favorable Therapeutic Index *in Vivo*. *Sci Transl Med* **2016,** *8*, 325ra17.
49. Camacho, K. M.; Menegatti, S.; Vogus, D. R.; Pusuluri, A.; Fuchs, Z.; Jarvis, M.; Zakrewsky, M.; Evans, M. A.; Chen, R.; Mitragotri, S., Dafodil: A Novel Liposome-Encapsulated Synergistic Combination of Doxorubicin and 5fu for Low Dose Chemotherapy. *J Control Release* **2016,** *229*, 154-162.
50. Nair, A. B.; Jacob, S., A Simple Practice Guide for Dose Conversion between Animals and Human. *J Basic Clin Pharm* **2016,** *7*, 27-31.
51. Fromen, C. A.; Robbins, G. R.; Shen, T. W.; Kai, M. P.; Ting, J. P.; DeSimone, J. M., Controlled Analysis of Nanoparticle Charge on Mucosal and Systemic Antibody Responses Following Pulmonary Immunization. *Proc Natl Acad Sci U S A* **2015,** *112*, 488-93.
52. Kai, M. P.; Brighton, H. E.; Fromen, C. A.; Shen, T. W.; Luft, J. C.; Luft, Y. E.; Keeler, A. W.; Robbins, G. R.; Ting, J. P.; Zamboni, W. C.; Bear, J. E.; DeSimone, J. M., Tumor Presence Induces Global Immune Changes and Enhances Nanoparticle Clearance. *ACS Nano* **2015**.